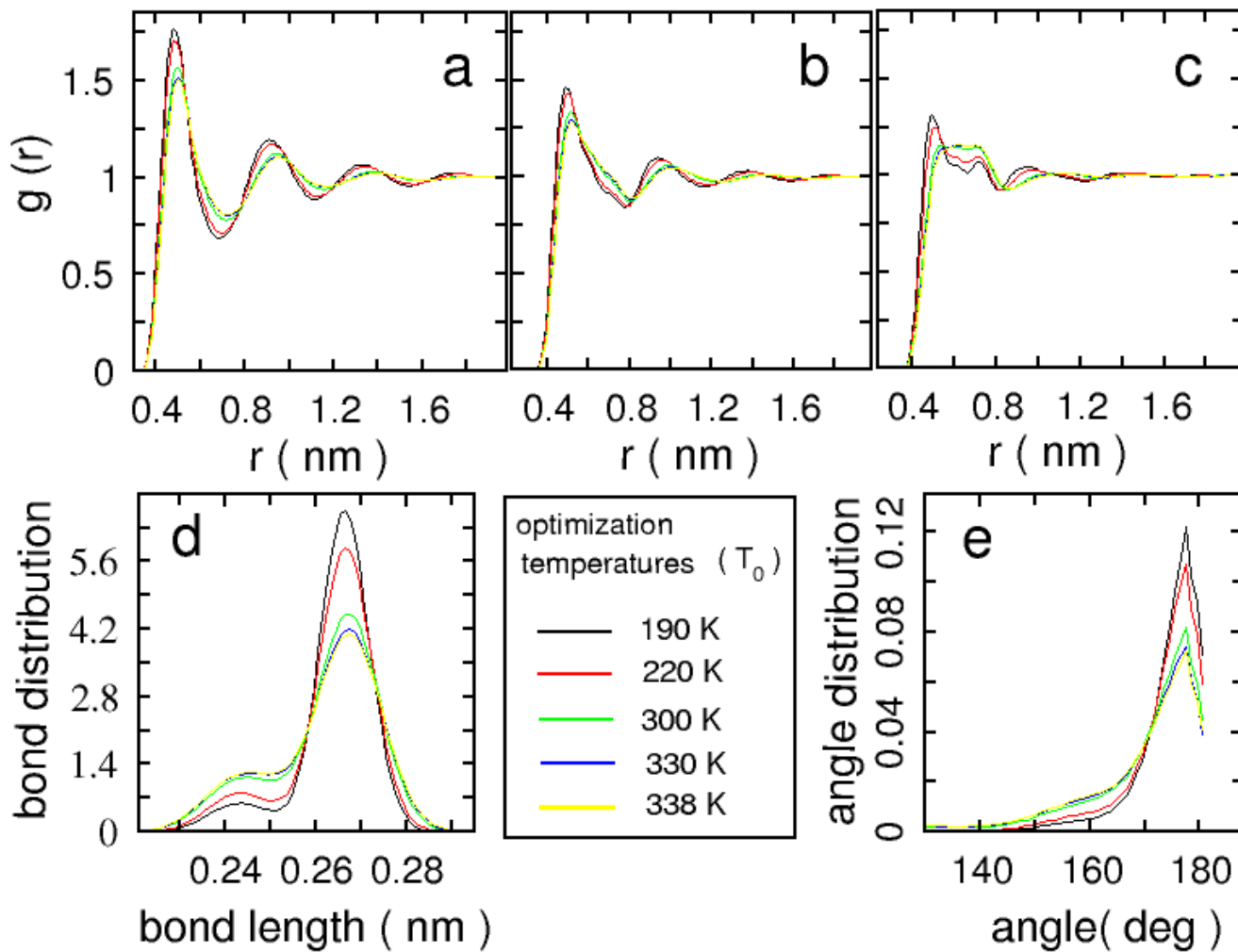
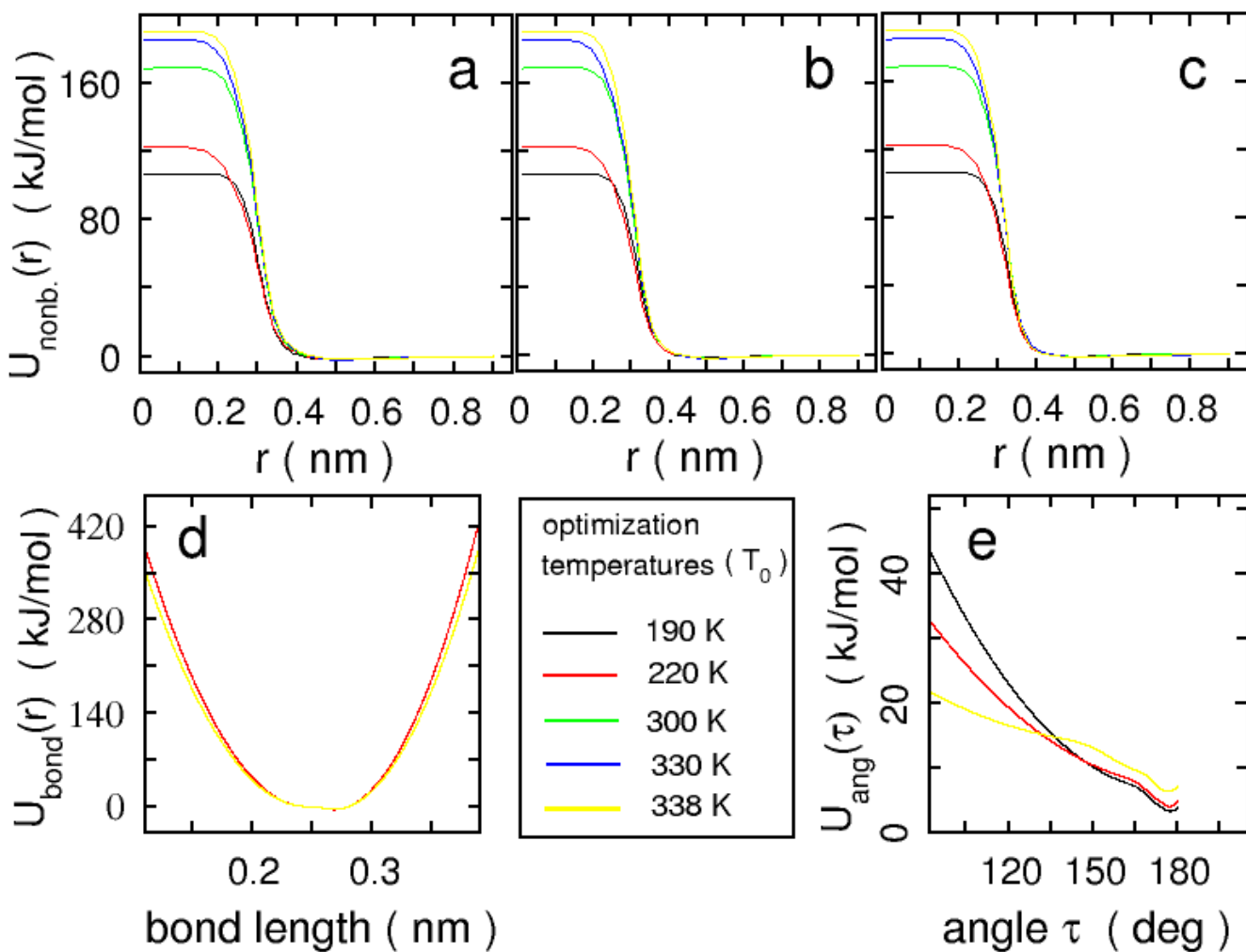


## Supporting Information



**Figure 1.** Target distribution functions calculated from the atomistic trajectories for five different optimization temperatures  $T_0$ . The mapping scheme employed is displayed in Fig.1 of the article. In diagrams a, b and c the target nonbonded radial distributions  $g(r)$  between the beads of type 1-1, 1-2 and 2-2 are shown. The target bond and angle functions are displayed in diagrams d and e.



**Figure 2.** Coarse-grained potentials resulting from the Iterative Boltzmann Inversion for the five optimization temperatures  $T_0$  considered. The mapping scheme employed is displayed in Fig.1 of the article. The diagrams a, b and c show the nonbonded potentials between the beads of type 1-1, 1-2 and 2-2. The bond and angle potentials are displayed in diagrams d and e. Note that the potentials in diagram a are different from the ones in b and c (even if this is not completely apparent from the plots). In diagram d the potentials optimized at  $T_0 = 300, 330$  and  $338$  K completely overlap. The same holds for the potentials optimized at  $190$  and  $220$  K. In diagram e the overlap is again between the potentials optimized at  $T_0 = 300, 330$  and  $338$  K.

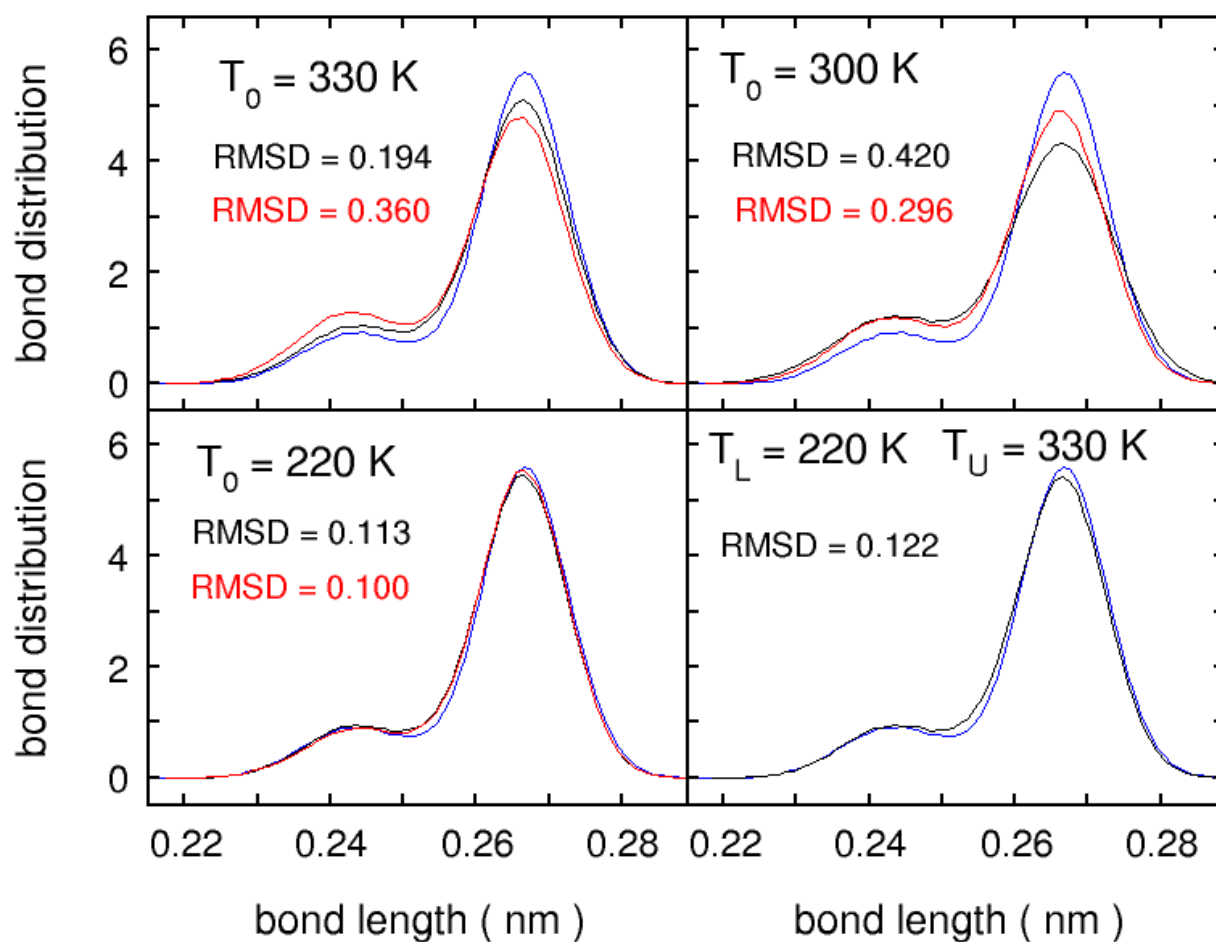


**Figure 3.** Comparison between the target bond distribution derived from the atomistic trajectory at  $T = 240 \text{ K}$  and the results of the different scaling methods. The curves are colored according to the coloring scheme in Fig. 6 of the article. Therefore, the target distribution derived at  $T = 240 \text{ K}$  is plotted in blue in all four diagrams of the figure. The black curve in the bottom-right diagram is the bond distribution resulting from the use of the 2-point interpolation. In the three other diagrams the black curves correspond to the direct use of the potentials ( $f(T) = 1$ ). The red curves are the output of the simulations in which the best factor  $f(T)$  for each  $T_0$  has been employed. The RMSD values between the target function and the simulated ones have been symbolized following the coloring scheme defined above.

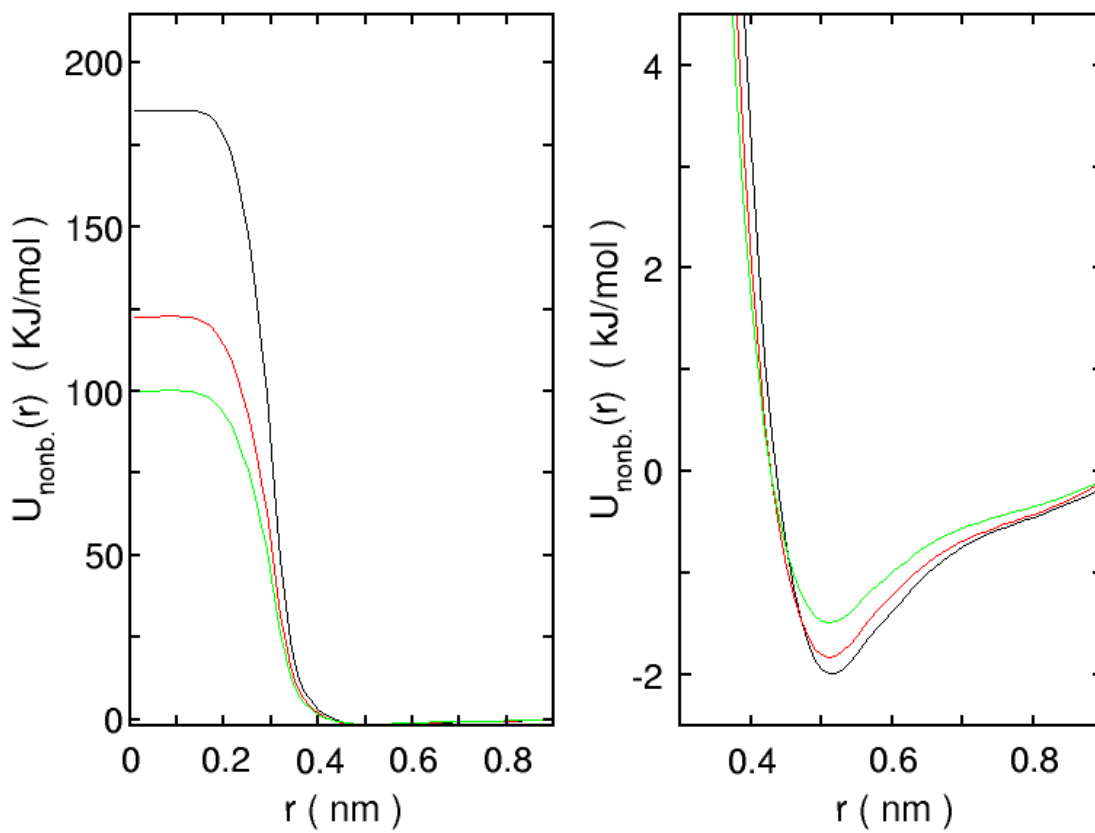


**Figure 4.** Effect of the scaling factor  $f(T) = (T_0 / T)^{1/2}$  on the nonbonded coarse-grained interaction potential between two beads of type 1 resulting from the IBI optimization. The same potentials are plotted in the left and right diagrams. The right one is zoomed to emphasize the curve shapes in the vicinity of the minimum. The black and red curves are the potentials optimized with the Iterative Boltzmann Inversion at 330 K and 220 K. The green curve is the potential resulting from the scaling process using  $f(T) = (T_0 / T)^{1/2}$  with  $T_0 = 220$  K and  $T = 330$  K (Eq. (1) of the article).

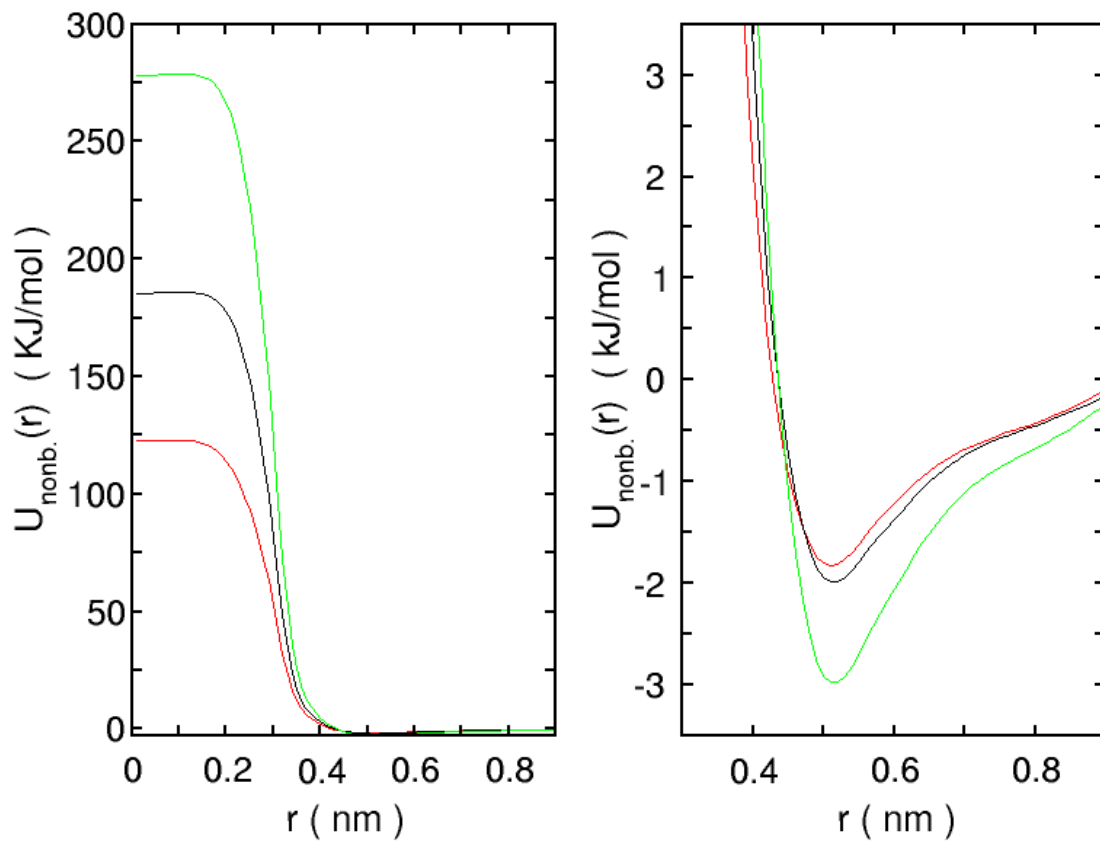


**Figure 5.** Effect of the scaling factor  $f(T) = T_0 / T$  on the nonbonded coarse-grained interaction potential between two beads of type 1 resulting from the IBI optimization. The same potentials are plotted in the left and right diagrams. In analogy with Fig. 4 the right one is zoomed. The black and red curves are the potentials resulting from the Iterative Boltzmann Inversion at 330 K and 220 K. The green curve is the potential resulting from the scaling process using  $f(T) = T_0 / T$  with  $T_0 = 330$  K and  $T = 220$  K (Eq. (1) of the article).

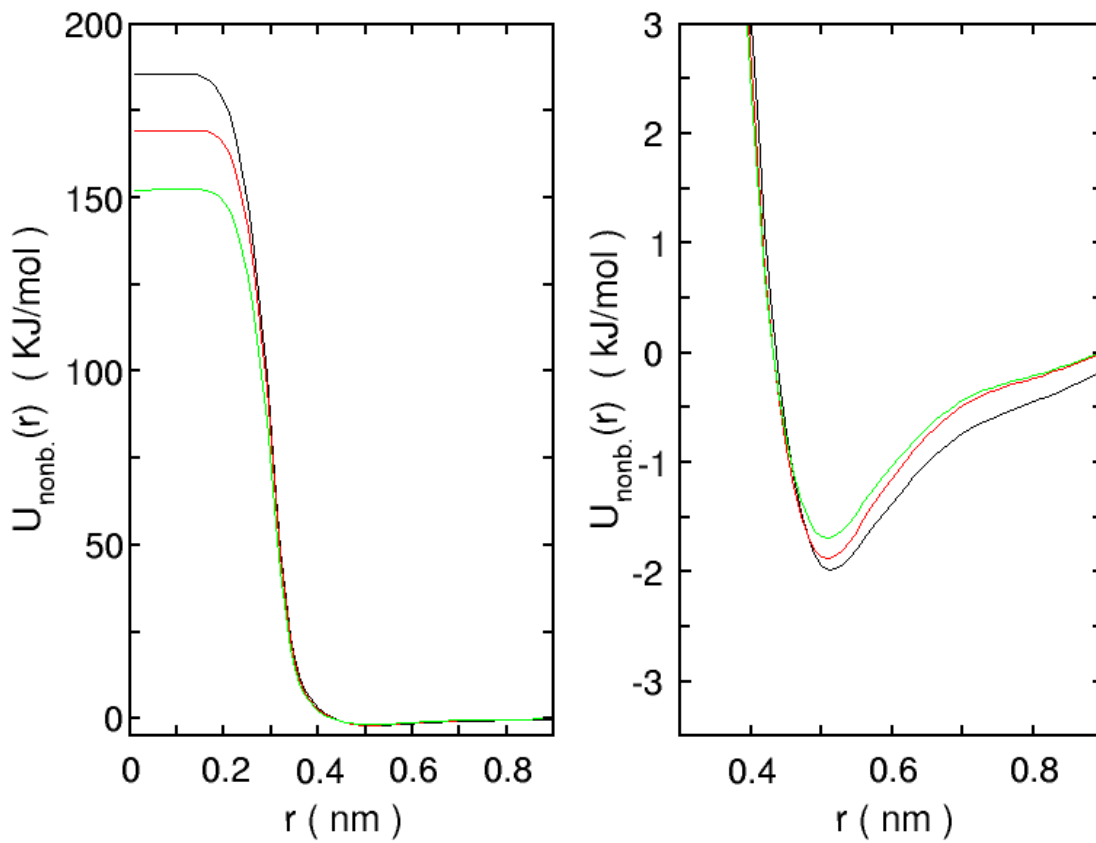


**Figure 6.** Effect of the scaling factor  $f(T) = T_0 / T$  on the nonbonded coarse-grained interaction potential between two beads of type 1 resulting from the IBI optimization. The same potentials are plotted in the left and right diagrams. In analogy with Fig. 4 the right one is zoomed. The black and red curves are the potentials resulting from the Iterative Boltzmann Inversion at 330 K and 300 K. The green curve is the potential resulting from the scaling process using  $f(T) = T_0 / T$  with  $T_0 = 300$  K and  $T = 330$  K (Eq. (1) of the article).

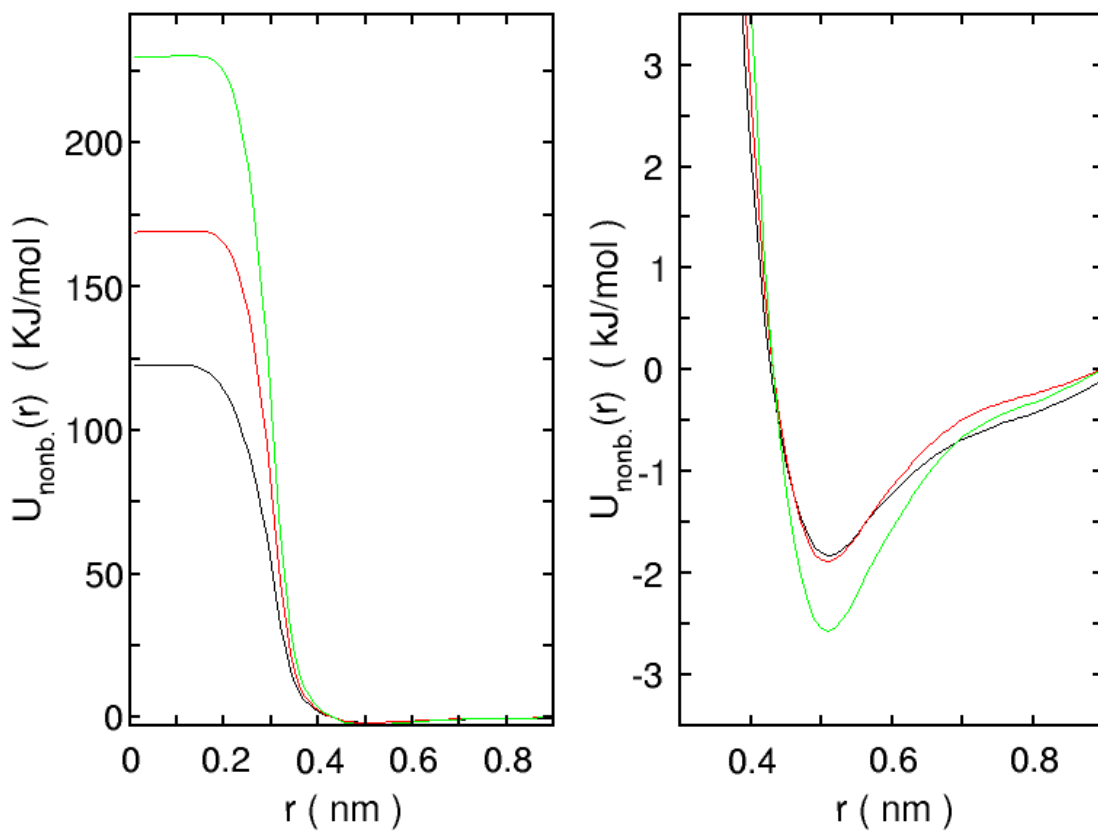


**Figure 7.** Effect of the scaling factor on the nonbonded coarse-grained interaction potential between two beads of type 1 resulting from the IBI optimization. The same potentials are plotted in the left and right diagrams. In analogy with Fig. 4 the right one is zoomed. The black and red curves are the potentials resulting from the Iterative Boltzmann Inversion at 220 K and 300 K. The green curve is the potential resulting from the scaling process using  $f(T) = T_0 / T$  with  $T_0 = 300$  K and  $T = 220$  K (Eq. (1) of the article).

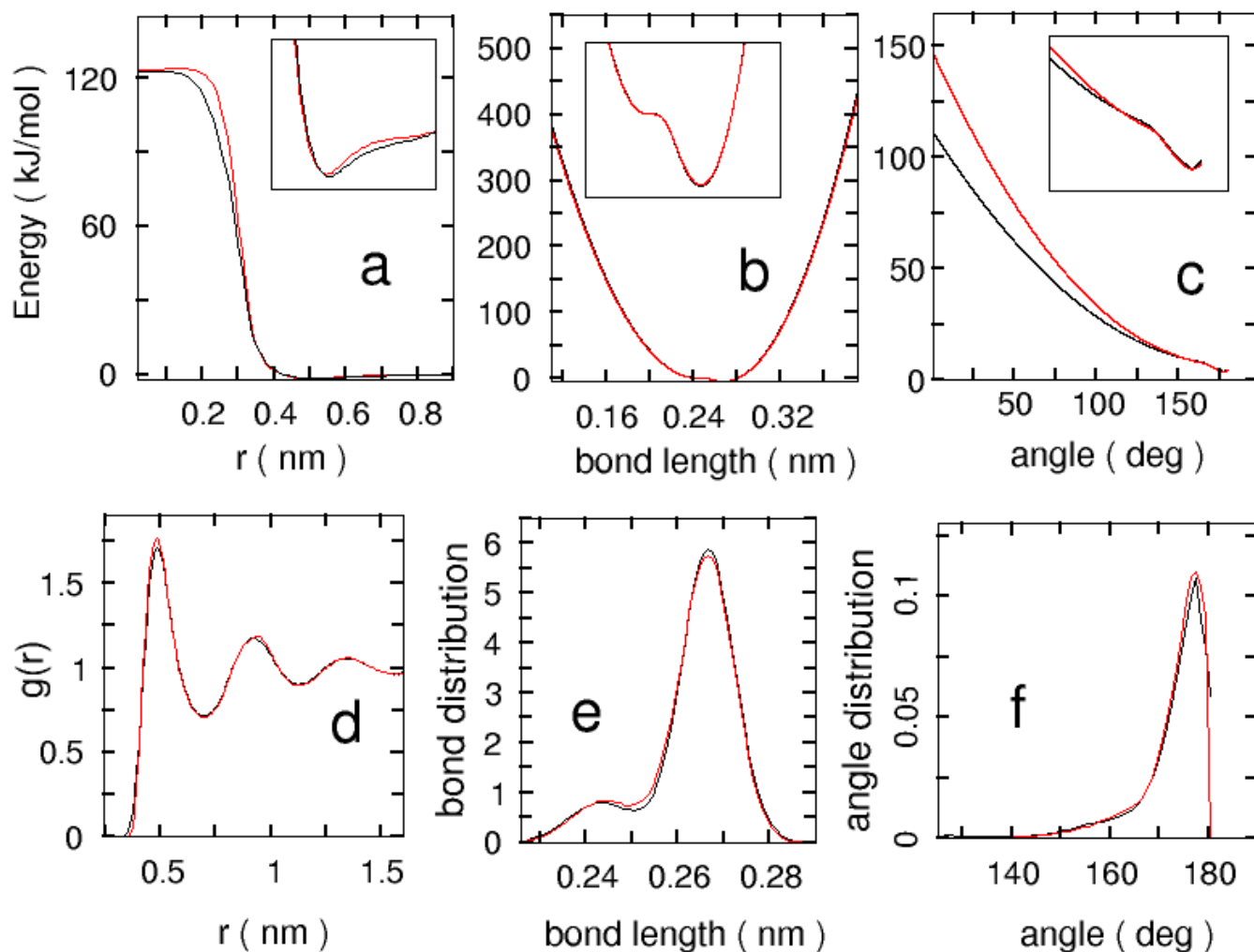


**Figure 8.** Comparison between the coarse-grained potentials obtained from the IBI optimization at 220 K (black curves in diagrams a, b and c) and the potentials generated for CG simulations at T = 220 K by the 2-point interpolation with  $T_L = 190$  K and  $T_U = 338$  K (red curves in the diagrams). The energy values of the nonbonded potential for two beads of type 1 (diagram a) and of the bond and angular potentials (b and c) are expressed in kJ/mol. The small pictures inserted in the three diagrams are only a zoom around the minimum of the potentials. In the diagrams d, e and f we have plotted the target distributions associated with the potentials mentioned above. These distributions are derived from the IBI optimization at 220 K (black curves) and from the simulation

which has used the CG potentials generated by the 2-point interpolation at  $T = 220$  K (red curves).

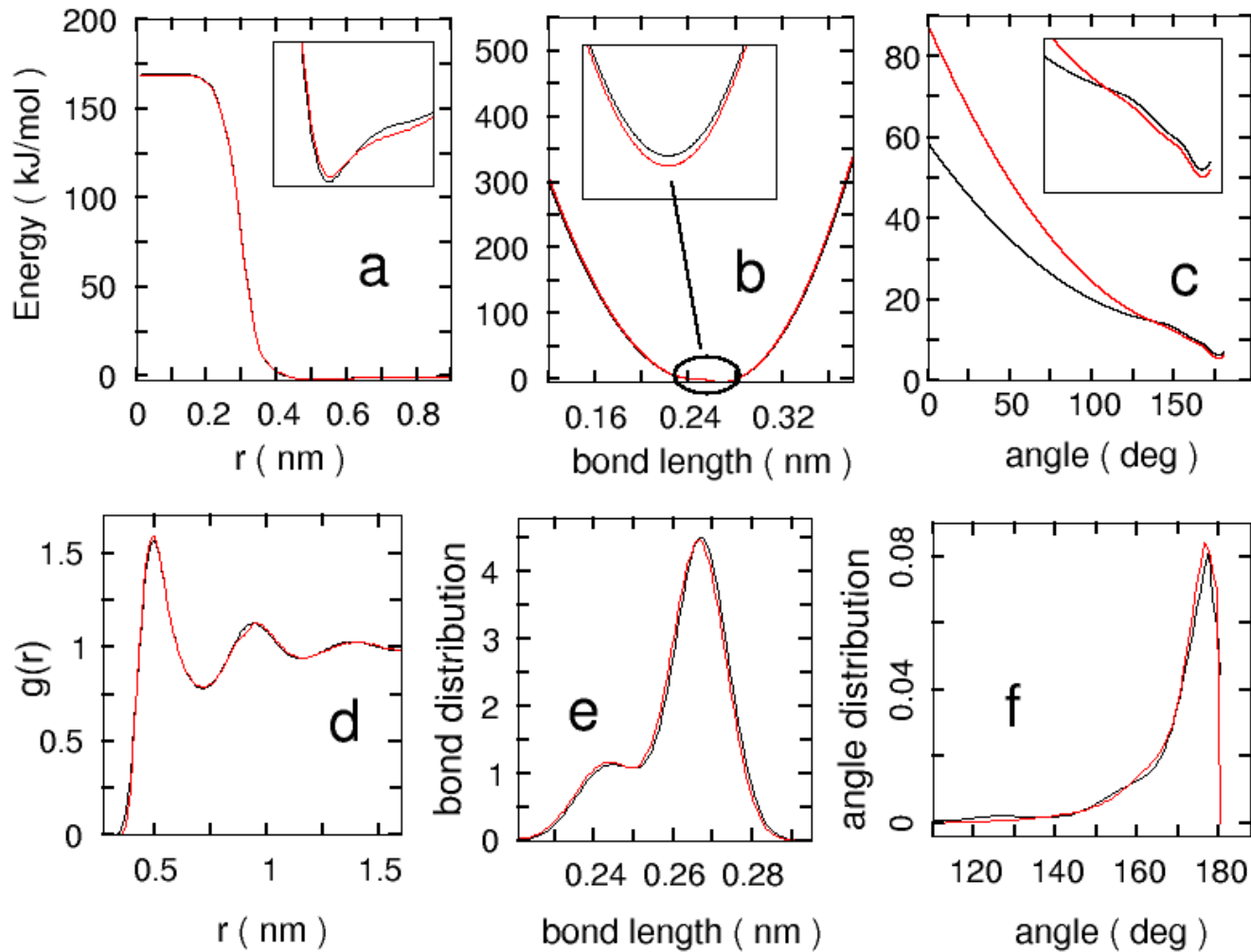


**Figure 9.** Comparison between the coarse-grained potentials obtained from the IBI optimization at 300 K (black curves in diagrams a, b and c) and the potentials generated for CG simulations at  $T = 300$  K by the 2-point interpolation with  $T_L = 190$  K and  $T_U = 338$  K (red curves in the diagrams). The energy values of the nonbonded potential for two beads of type 1 (diagram a) and of the bond and angular potentials (b and c) are expressed in kJ/mol. The small pictures inserted in the three diagrams are only a zoom

around the minimum of the potentials. In the diagrams d, e and f we have plotted the target distributions associated with the potentials mentioned above. These distributions are derived from the IBI optimization at 300 K (black curves) and from the simulation which has used the CG potentials generated by the 2-point interpolation at T = 300 K (red curves).